frontiers | Frontiers in Space Technologies

TYPE Original Research
PUBLISHED 27 September 2023
DOI 10.3389/frspt.2023.1255535

OPEN ACCESS

EDITED BY
Beth Lomax,
European Space Research and Technology Centre (ESTEC), Netherlands

REVIEWED BY
Aliz Zemeny,
European Space Agency (ECSAT), United Kingdom
David Karl,
Technical University of Berlin, Germany

*CORRESPONDENCE
Jared M. Long-Fox,
jared.long-fox@ucf.edu

RECEIVED 09 July 2023
ACCEPTED 14 September 2023
PUBLISHED 27 September 2023

CITATION
Long-Fox JM and Britt DT (2023), Characterization of planetary regolith simulants for the research and development of space resource technologies.
Front. Space Technol. 4:1255535.
doi: 10.3389/frspt.2023.1255535

Characterization of planetary regolith simulants for the research and development of space resource technologies

Jared M. Long-Fox* and Daniel T. Britt

Department of Physics, University of Central Florida, Orlando, FL, United States

Human planetary exploration and colonization efforts are reliant on the ability to safely interact with planetary surfaces and to leverage local regolith as a resource. The high-cost and risk-intensive nature of establishing planetary infrastructure and resource utilization facilities necessitates risk reduction through laboratory-based research and development of space resource acquisition, processing, and extraction technologies using appropriate, well-characterized, mineral-based regolith simulants. Such simulants enable the planetary exploration and resource utilization communities to test large-scale technologies and methodologies for a relatively low cost as an alternative to scarce and expensive returned samples. The fidelity of a regolith simulant for any application is, in part, determined by the mineralogical composition and particle size distribution. The importance of composition is well established for *in situ* resource utilization studies sensitive to geochemical properties but tends to be ignored in studies concerned with physical properties. Neglecting to consider mineralogy reduces the fidelity of a simulant since each mineral species has its own unique grain density, preferred grain geometry, and intergranular forces, all of which affect the physical properties of the simulant (e.g., shear strength, bearing strength, bulk density, thermal and electrical properties, magnetic properties). Traditionally, regolith simulants have been limited in quantity and availability; Exolith Lab remedies these problems by designing simulants in a constrained maximization approach to fidelity relative to cost, material availability, and safety. Exolith Lab simulants are designed to approximate the mineralogy and particle size ranges of the planetary regolith being simulated, with composition constrained by remote sensing observations and/or returned sample analyses. With facilities and equipment capable of high-volume simulant production, Exolith Lab offers standard simulants in bulk that are readily available for purchase and shipment. This work reviews the production methods, equipment, and materials used to create Exolith Lab simulants, provides compositional data, particle size data, and applications for each standard lunar, Martian, and asteroid simulant that Exolith Lab offers.

KEYWORDS

regolith simulant, mineralogy, physical properties, planetary exploration, SRU, space technology, laboratory testing

1 Introduction

Humans are turning their eyes to the sky more than ever before with an increased interest in space exploration and the resources we can obtain from planetary bodies to fuel the advancement of humanity into a space-faring species. As this interest in planetary exploration and resource utilization increases, the need to develop and test technologies ranging from in-space propellant production (Kornuta et al., 2019), mobility systems (Colaprete et al., 2019), resource acquisition (Just et al., 2020), extraction (Guerrero-Gonzalez and Zabel, 2023), transport/conveyance (Cannon et al., 2022), and infrastructure development (Thangavelauthan and Xu, 2022) systems using appropriate simulants also increases. It is not feasible to launch bulk resources and equipment to space to perform operations on the surface of the Moon, Mars, and asteroids, so local resources will need to be used, namely, planetary regolith (Sanders et al., 2022). Planetary regolith is the layer of loose rock and sediments that covers bedrock on planetary surfaces, such as the Moon and Mars (McKay et al., 1991). Since planetary regolith is composed of geologic materials (minerals, amorphous glasses, native elements, etc.), it can be used in space resource utilization (SRU) and/or *in situ* resource utilization (ISRU). NASA's Apollo missions returned both regolith and rock samples from the Moon (e.g., Schmitt et al., 1970), the NASA/ESA Mars Sample Return mission (Kminek et al., 2022) is planning on returning the first Martian samples in 2033, and asteroid sample return missions are underway (Walsh et al., 2022) with Hayabusa2 already returning to Earth (Watanabe et al., 2019; Yada et al., 2022), but none of these provide sufficient amounts of material to test and develop SRU and ISRU technologies. In this absence of abundant bulk returned regolith samples, technologies aimed for use on the surfaces of the Moon, Mars, or asteroids must be tested with terrestrially-derived simulated planetary regolith (simulants). The more closely these simulants approximate the regolith they are created to simulate, the better the quality of studies and testing. Previous simulants have generally disregarded mineralogical accuracy as a necessary design component, but this is in error since the mineralogical composition of geologic materials determine not only the geochemical properties of the simulant, but also the thermal, electrical, mechanical properties. Exolith Lab offers solutions to the planetary science and engineering communities through the bulk manufacture of mineralogically accurate lunar, Martian, and asteroid regolith simulants (Figure 1). This work details the design philosophy, design process, and manufacturing processes used to create Exolith Lab simulants as well as motivation, background, use cases, mineralogical compositions, bulk elemental compositions (in equivalent oxides) from wavelength dispersive x-ray fluorescence (XRF) data, compositional phase information from x-ray diffraction (XRD) data, and particle size distribution (PSD) at the time this work was authored. The goal of this work is to

FIGURE 1
Exolith Lab planetary regolith simulants **(A)** LHS-1, **(B)** LMS-1, **(C)** LHS-1D, **(D)** LMS-1D, **(E)** MGS-1, **(F)** MGS-1C, **(G)** MGS-1S, **(H)** JEZ-1, **(I)** CI-V2, **(J)** CM-V2, and **(K)** CR-V2.

FIGURE 2
(A) Sieves and sieve shakers used in small-batch Exolith Lab simulant production, **(B)** sieves and sieve shaker used in bulk, large-volume Exolith Lab simulant production, **(C)** hammer mill and **(D)** jaw crusher used to percussively crush rocks and minerals for use in Exolith Lab simulants, **(E)** cement mixer with steel balls added for ball milling simulants to particle sizes smaller than the Exolith Lab hammer mill and jaw crusher can produce, **(F)** cement mixers used to mix simulant and serve as ball mills when steel balls are added during mixing.

describe the philosophy and capabilities of Exolith Lab and the current main production line of lunar, Martian, and asteroid regolith simulants and establish the simulants themselves, the design philosophy, characterization methods, and the production methods as open-source standards for testing of any technology or system intended for extraterrestrial use. Forthcoming work will perform quantitative analyses on each of these simulants to compare their physical and chemical properties to the regolith they are intended to simulate, and as such, detailed comparisons are not directly provided here.

The mineralogic compositions of Exolith Lab simulants are based on returned samples and remote sensing data. Once the mineralogy of the target body or site is estimated, Exolith Lab finds terrestrial rocks and minerals with well-characterized, reliable sources to provide materials that either arrive pre-processed to specific grain size ranges or uses in-house rock crushing equipment to crush feedstock and size sort using ASTM standard sieves and sieve shakers (Figures 2A, B). To better simulate the irregular, jagged shapes of lunar and asteroid regolith grains that result from undergoing space weathering processes over billions of years, Exolith Lab strives to attain realistic grain shapes by using percussive crushing methods (hammer mill and jaw crusher, Figures 2C, D). When simulants with small (e.g., less than ~50 μm) maximum particle sizes are being produced, ball mills (Figure 2E) are used to reduce particle size to the desired range. Once each mineral or rock is prepared, the constituents are combined in the desired proportions (with <0.5 wt% difference in each production run) and mixed in cement mixers (Figure 2F).

When discussing the chemical composition of geologic materials, it is not sufficient to only describe the mineralogy since different minerals can have varying concentrations of elements and often exist on compositional continua (e.g., solid solutions). Since planetary regolith is created from different materials and in different environments from that of Earth, the relative concentrations of elements within minerals and the form those elements take (e.g., native elements, oxides, glasses, or minerals) vary widely. This means that there is a definitive need for determination of the bulk elemental composition of returned regolith and simulants to be able to accurately compare geochemical properties of simulant used for research and development of ISRU- and exploration-related technologies. The trace element profile of a regolith simulant is inherently the trace element profile of a terrestrial material since simulants are created solely from materials found on Earth, and since planetary terrestrial regolith formation processes are vastly different, a simulant should never be correlated to actual planetary regolith in trace element analyses. Here, the major and minor elemental

composition of Exolith Lab simulants is given as equivalent oxides based on XRF analysis. Comparisons to lunar, Martian, and asteroid XRF data are not provided here since this work is specifically a description of simulants, design philosophy, and characterization and production methods, but forthcoming publications should provide detailed comparisons to actual planetary regolith XRF data.

The compositional phases of planetary regolith are highly varied and impacted by weathering processes that mechanically and chemically alter the rocks and minerals on the Moon, Mars, and asteroids. Knowledge of the proportions of different mineralogic and amorphous phases present of planetary regolith provides insights into formational and evolutionary processes that affected or are still affecting the regolith in question, and this determines the processing needed to be able to use the regolith as a resource or a construction material. Even though Exolith Lab uses a mineral-based design philosophy that utilizes high-purity materials combined in specific proportions to make planetary regolith simulants, characterizations of the different compositional phases is key to the research and development of space resource technologies. Such characterizations allow comparison to planetary samples either returned or impacted onto Earth or *in situ* mineralogical/phase measurements on other planetary bodies to better understand results obtained in testing space resource technologies using a given simulant and how the simulant can be improved if new data is obtained. If simulants used in laboratory testing of space resource technologies are well characterized in terms of phases present, results from laboratory testing can provide information on the most efficient way to utilize planetary regolith and how planetary regolith weathering processes affect *in situ* regolith. As with XRF data, direct comparisons of XRD data between Exolith Lab lunar, Martian, and asteroid simulants are not given here because the intent of this paper is to formally introduce and describe the simulants presented and forthcoming publications should provide rigorous, quantitative comparisons between simulants and regolith.

The particle size range and distributions determine the physical (thermal, electromagnetic, and mechanical) and chemical properties of planetary regolith, therefore simulants should match the particle size ranges and distributions of the regolith they are intended to simulate. Since the ease and cost of space exploration, resource prospecting, mining, and processing are all so dependent on being able to operate in extreme conditions with planetary particle size ranges and distributions, technologies must be tested and validated prior to flight in appropriate testing materials with realistic compositions and particle sizes. Since particle size and PSD strongly affect the physical properties of a regolith, these properties were ranked as the top two most important properties that a regolith simulant must match (Sibille et al., 2006). Exolith Lab controls particle size range of produced simulants at the processes level with the goal to replicate the particle size range and distribution of the <1 mm size fraction of lunar and Martian regolith. Asteroid simulants are available in fine powder (<1 mm) or "cobble" (coarse aggregate) form (terminology from Britt et al., 2019), with the "cobble" form having a larger particle size range and more variable PSD with aggregates ≥10,000 μm (1 cm). Throughout this work, the geoscience standard Wentworth (1922) particle size scale and nomenclature is used for all size descriptions, and by this scheme, the "cobble" nomenclature for asteroid simulants established by Britt et al. (2019) is formally "pebbles."

2 Materials and methods

2.1 Simulant production methods

2.1.1 Design philosophy

Exolith Lab simulant design and manufacturing philosophy is a constrained maximization of fidelity relative to cost, safety, and material availability, and parameters tuned in this optimization are mineralogy and particle geometry (size and shape). Mineralogy is a cornerstone of Exolith Lab's design philosophy because mineralogy determines the geochemical and physical properties since each mineral has a unique crystal habit, cleavage planes, chemistry, and grain density. Particle size range and distribution are among the most important aspects of lunar and planetary regolith simulants (Sibille et al., 2006; Metzger et al., 2019) as they drive geomechanical properties as well as affecting material processing requirements for ISRU (e.g., melting temperatures for metal and oxygen extraction, material transport). Based on the contributions of these factors to the physical and chemical properties of planetary regolith, mineralogy and particle geometry are highly important factors that need to be considered in simulant selection for research and development efforts in mobility, dust mitigation, tool-regolith interactions, resource evaluation, resource acquisition, material transport, resource extraction and refinement, and infrastructure development.

2.1.2 Material sourcing and simulant production equipment

Exolith Lab sources bulk amounts of high purity commercially available rocks and minerals for use in simulant production. Procuring large amounts of material not only enables more simulant to be produced without downtime waiting for material to arrive, but it also provides higher product consistency. Where possible, constituents that have been or are currently being used in other commonly used simulants are being used, such as Merriam crater basalt that was used in JSC-1 (McKay et al., 1994) and Greenspar anorthosite. The use of Merriam crater basalt in Exolith Lab simulants is a recent change at the time of writing (and was used in the simulants analyzed and presented in this work), and this specific change was made to be more directly comparable to other simulants. Even though Exolith Lab aims to keep material sources and production methods consistent as possible, sometimes change is necessary due to inevitable issues such as a change in material source location (even different sites within the same mine, for example,), material supplier, or equipment upgrades. Such material changes affect the simulant by altering things such as (but not limited to) chemical composition, processing requirements that can affect particle shape and size distributions, and grain density. Exolith Lab works to keep feedstock as consistent as possible though direct connections with suppliers and changing only when material becomes unavailable or it drastically affects price and there is a suitable alternative readily available, though quantitative analysis on variation of simulant mineralogy and particle size distribution is not performed through time. Information on materials and material sources used in simulants can be requested by contacting Exolith Lab and providing information on when the simulant was purchased. For the most up-to-date information on Exolith Lab simulants, custom simulant

creation, or scientific simulant consultations, please visit the Exolith Lab website (www.exolithsimulants.com).

2.2 Data collection methods

2.2.1 XRF

XRF is an accepted method for the accurate quantification of the bulk elemental composition of geologic materials (e.g., Hooper, 1964) is widely applied to analysis of extraterrestrial material *in situ* (Adler et al., 1972a; Adler et al., 1972b; McKenzie et al., 2020), in laboratories (Rose et al., 1970), and evaluating simulant suitability for testing ISRU and exploration technologies (Isachenkov et al., 2022). Using a method similar to Johnson et al. (1999), the Hamilton Analytical Laboratory (HAL) at Hamilton College performed XRF analysis on Exolith Lab simulants to determine their bulk elemental composition and trace element abundances. These XRF data were acquired using low dilution fused bead method with graphite crucibles. Samples were ground in a tungsten carbide ring mill and the powder was then combined in a 2:1 flux:powder ratio. This mix was then blended and fused in a graphite crucible at 1,000°C. The resulting pellets were cleaned of residual carbon and then reground and refused again at 1,000°C. The surfaces of the doubly fused pellets had their surfaces finished (15 μm surface finish) and cleaned in ethanol. The prepared samples were then analyzed in the Thermo ARL Perform'X spectrometer with an accelerating voltage of 45 kV and 45 mA current. Loss on ignition (LOI) was measured for all samples by heating 15–17 h in silica crucibles at 900 °C. This temperature is chosen to allow any organic matter, carbonates, and other volatiles to be baked off while minimizing the loss of sodium, potassium, and lead, and the duration of heating is chosen to more complete oxidation of iron to a single oxidation state. The differences of the low dilution graphite fusion method include: 1) a single sample allows for major, minor, and trace elements to be analyzed, increasing efficiency without a loss of accuracy; 2) a constant voltage on an Rh target is used to achieve stability and precision for all elements; 3) the oxidation state of iron and the volatile content of the rocks and minerals being analyzed is disregarded, leaving the major element concentrations to be reported as normalized and free of volatiles with all iron expressed as FeO rather than split into Fe_2O_3 and FeO (Johnson et al., 1999). More information on the sample preparation and analysis procedure can be found in Johnson et al. (1999) and at https://www.hamilton.edu/academics/analytical-lab.

2.2.2 XRD

XRD is an analytical technique often used to identify different phases in crystalline materials (Bunaciu et al., 2015) and is hence often used to characterize the different minerals and amorphous material present in rocks and minerals, whether terrestrial or from space such as meteorites (Bland et al., 2004) or returned lunar samples (Taylor et al., 2019). The Engineering and Mining Experiment Station (EMES) at the South Dakota School of Mines and Technology used a Malvern Panalytical Empyrean x-ray diffractometer with a cobalt cathode (λ = 1.79 Å) at 40 kV accelerating voltage and 45 mA current to generate x-ray diffraction patterns for Exolith Lab lunar, Martian, and asteroid simulants. iCore and dCore automated optics using fixed slits approximately 1 cm × 1 cm footprint were normal to the beam and a PIXcel3D detector was operated as a scanning line 1D detector. The samples of simulant were crushed with a ball mill and mixed with 10%–15% corundum as an internal standard for amorphous content determination. Samples were scanned in values of 2θ from 5° to 90° at a rate of 0.3° per second with five iterative rotations and subsequent re-scans of the sample to assist in reducing texture contributions from the wide PSDs of the simulants. Phase identifications are not offered here since Exolith Lab simulants are created using specific proportions of well-documented mineral and rock components so the input mineralogy is known. XRD data presented here are available upon request to allow Exolith Lab and other simulant users to compare the phase compositions before and after working with simulants at extreme temperatures or pressures that cause phase changes such as metal and oxygen extractions. It should be noted that XRD patterns are best when the material being analyzed is of uniform particle size, but Exolith Lab simulants often have particle size ranges that span at least four orders of magnitude (and often more), which lowers overall peak intensity in XRD patterns, potentially rendering phase identification difficult, and even proper sample preparation methods may not fully resolve this. More information on XRD data collection and analysis can be found at https://www.sdsmt.edu/EMES/.

2.2.3 Particle size analysis

The PSDs of Exolith Lab simulants were measured by a CILAS 1190 volumetric particle size analyzer (0.04–2,500 μm detection range) in liquid dispersion mode using deionized (DI) water as the dispersal agent. To analyze simulant samples, the simulant was added to the vibrating dispersal cell and then was pumped to the measurement cell. In the measurement cell, lasers of 640 and 830 nm wavelengths strike incident in the suspended particles and diffract onto detectors. The CILAS 1190 uses the CILAS Size Expert software pipeline to analyze the diffraction patterns of the three independent samples of each simulant being tested, and the volumetric percentages of each size bin, or the density function (q3), and the cumulative distribution (Q3) are calculated for each of the three samples of each simulant. From these samples, the mean of both the density functions and cumulative distributions are calculated with 2σ confidence intervals. From the cumulative distribution, the D10, D30, D50, D60, and D90 particle sizes are calculated along with the span (*s*, Eq. 1) of each distribution. D10 is the particle size at which 10% of the volume of particles in the distribution are smaller than that size, and D30 is the particle size at which 30% of the volume of particles in the distribution are smaller than that particular size, D50 is the median size, D60 is the size at which 60% of the particles are volumetrically smaller, and D90 is the size at which 90% of the particles are volumetrically smaller than that size. These values are also used to calculate the coefficient of uniformity (C_u, Eq. 2) and the coefficient of curvature (C_c, Eq. 3) to serve as another standard metric to describe PSDs as described in ASTM D2487 (ASTM Standard D2487 2017).

$$s = \frac{D90 - D10}{D50} \tag{1}$$

$$C_u = \frac{D60}{D10} \tag{2}$$

$$C_C = \frac{(D30)^2}{D10 \times D60} \tag{3}$$

It should be noted that the binding agent used to produce the pebble-sized asteroid simulants from the powder simulants is soluble in water and the cobbles are relatively weak, so the asteroid simulant PSDs reported here are only representative of the loose powder forms of each asteroid simulant. Comparisons to particle size data from lunar, Martian, and asteroid regolith are not made here, for the same reasons stated before regarding XRF and XRD data: this manuscript serves only to introduce and describe the simulants with rigorous quantitative comparisons recommended for future publications describing the Exolith Lab simulants discussed here.

2.3 Lunar regolith simulants

The lunar regolith is formed from physical and chemical space weathering processes, such as impact gardening and solar irradiation, that break down the lunar bedrock (Hörz et al., 1991). The hard vacuum on the surface of the Moon is a strongly reducing environment, presenting phenomena and compositions that are not observed on Earth (Taylor et al., 2001). The lunar surface can be broken down into two main geologic provinces: the feldspathic lunar highlands which cover 80% of the lunar surface and the basaltic lunar mare (Haskin and Warren, 1991; Spudis and Pieters, 1991; Head and Wilson, 1992; Jolliff et al., 2000). Aside from the lunar highlands and mare, there are more less commonly observed geologic domains including silicic volcanic features that are similar to terrestrial rhyolitic domes (Head and McCord, 1978; Hagerty et al., 2006; Siegler et al., 2023) as well as pyroclastic deposits (Gaddis et al., 2003; Gustafson et al., 2012; Trang et al., 2017). The lunar highlands comprise the original crust formed through differentiation during the formation of the Moon and are dominantly composed of anorthosite and similar lithologies (Crites and Lucey, 2015; Taylor et al., 2019). The lunar mare formed when ancient basaltic magma originating in the lunar mantle ascended, erupted as lava, and flowed to fill topographic lows such as impact basins (Taylor et al., 1991; Head and Wilson, 1992). These two generalized geologic provinces were explored by NASA's Apollo missions which returned samples from highlands, mare, and areas near the contacts between the highlands and mare. The compositions of regolith samples from the margins between the highlands and mare show intermediate compositions that indicate mixing of the regolith from both provinces (e.g., Heiken and McKay, 1974), with material being transported as impact ejecta and subsequently impact gardened. Renewed efforts from organizations across the globe, including government space agencies, private companies, and more, aim to explore the lunar surface and establish permanent infrastructure, with the initial target being the lunar south pole. The south pole is shown to have a highlands-like composition (Lemelin et al., 2022) and contains some of the purest anorthosites (nearly 100% plagioclase) on the lunar surface (Ohtake et al., 2009). From the lunar south pole, crewed and autonomous activities will extend north and include various mare terranes, including KREEP mare basalts that are enriched in valuable and useful elements such as potassium (K), rare earth elements (REE), uranium, thorium, and phosphorus (P) (Carlson and Lugmair, 1979; Wieczorek and Phillips, 2000). With this renewed interest in sustained human and robotic presence on the lunar surface, technologies must be researched, developed, and tested using appropriate simulants on Earth to leverage the various compositions of the lunar regolith to maximize the safety and efficiency of various lunar systems.

Exolith Lab produces two main lunar regolith simulants that are designed to approximate the mineralogy and particle geometries of the lunar highlands and lunar mare regolith: LHS-1 (Figure 1A) simulates the lunar highlands, and LMS-1 (Figure 1B) simulates the lunar mare. Both of these simulants have a maximum particle size of 1,000 μm. Two "dusty" versions of each of these simulants are also offered, dubbed LHS-1D (Figure 1C) and LMS-1D (Figure 1D), and these have maximum particle sizes of ~35 μm ("clay" to "coarse silt" when classified by the Wentworth scale) and the same mineralogic composition of LHS-1 and LMS-1, respectively. The mineralogy of LHS-1 (and therefore LHS-1D) is based on the 90 to 1,000 μm portion of the particle size distribution of Apollo sample 67,461 (Simon et al., 1981), whereas LMS-1 (and therefore LMS-1D) was created based on Apollo sample 24,999 (Simon et al., 1981). As shown in Long-Fox et al. (2023), the PSD of LHS-1 and LMS-1 align well with "key" returned samples from the lunar highlands and mare, respectively, identified in the *Lunar Soils Grain Size Catalog* (Graf, 1993). LHS-1D and LMS-1D are designed to mimic the chemistry and mechanics of the finest portions of the lunar highlands and mare regolith and are manufactured by ball milling the "parent" LHS-1 and LMS-1 simulants. The clay/coarse silt-sized particles that make up LHS-1D and LMS-1D have high surface area to volume ratios, and as such, LHS-1D and LMS-1D are prone to electrostatic clumping (as seen at the base of the piles of simulant in Figures 1C, D) and other electrostatic and atmospheric effects that are not observed in LHS-1 and LMS-1 (Easter et al., 2022; Madison et al., 2022; Millwater et al., 2022).

2.4 Martian regolith simulants

The Martian regolith is produced by dynamic geologic processes, both past and present, including meteoritic impacts, eolian and fluvial processes, and volcanic activity (McCauly, 1973; Malin and Edgett, 2000; Murchie et al., 2009). Remote sensing observations indicate a global basaltic crust (McSween et al., 2009) that is processed into a globally distributed basaltic regolith (Yen et al., 2005), and three of the seven sites that have been directly sampled *in situ* by landers or rovers show similar basaltic mineralogy and bulk elemental compositions (Yen et al., 2013) with site-specific enrichments in other compositions (e.g., different volcanic and alteration products). It can be assumed that variation from this apparent global basaltic composition is driven by local geologic and environmental processes. The fine particles in the Martian regolith are lofted through various processes and entrained in atmospheric pressure systems that, just like on Earth, distribute these particles around the planet (Toon et al., 1977). The Rocknest site within Gale crater, the most well-characterized regolith on the Martian surface (Bish et al., 2013; Blake et al., 2013; Leshin et al., 2013; Achilles et al., 2017; Sutter et al., 2017), is composed of atmospherically distributed dust, and therefore can be expected to serve as a global average for the composition of the Martian regolith, despite the relative sulfur enrichment of the Curiosity landing region. The similarity of the

Rocknest regolith to the regolith of other landing sites makes it suitable to serve as the basis for mineralogically accurate Martian regolith simulants (Cannon et al., 2019).

Exolith Lab produces four Martian regolith simulants, all based on the Rocknest regolith with some supplementary contribution from remote sensing observations (e.g., Baird et al., 1976; Poulet et al., 2008). MGS-1 (Figure 1E) is the base simulant for the rest of the Martian simulants that Exolith Lab offers and was created to simulate Rocknest (Cannon et al., 2019) and hence the expected global average Martian regolith. The other Martian regolith simulants, MGS-1C (Figure 1F), MGS-1S (Figure 1G), and JEZ-1 (Figure 1H) use MGS-1 as the base component but add other mineral phases such as clay minerals and alteration products to simulate different areas of the Martian surface. MGS-1C is a modified version of MGS-1 that maintains the basaltic base component (plagioclase, olivine, and pyroxenes) but use enriched in clay minerals to simulate a clay-rich Noachian regolith. Due to the high-clay content, MGS-1C has a smaller median particle size than the rest of the Exolith Lab Martian regolith simulants. MGS-1S also maintains the root Rocknest-like composition but is amended with sulfate-rich minerals to mimic regolith found in a hydrothermally active zones on the Martian surface. Finally, JEZ-1 is the Exolith Lab simulant that approximates the expected mineralogy of Jezero crater, the site being sampled by NASA's Mars Sample Return mission that has strong mineralogical and geomorphic indications of a dynamic fluvial and lacustrine past (Horgan et al., 2020). Due to the inclusion of secondary minerals beyond the base MGS-1 composition, MGS-1C, MGS-1S, and JEZ-1 have PSDs that are multi-modal with the non-crystalline silicate phases being of larger grain size (~10–1,000 μm) and the additional, weathered/altered phases being a distinct smaller size fraction (~2–11 μm).

2.5 Asteroid regolith simulants

Asteroids, relative to other planetary bodies, are primitive objects that provide information on the nebula from which they formed, the materials that planets formed from and subsequently differentiated, cratering processes, space weathering processes (e.g., Clark et al., 2002), cratering, thermal and aqueous alteration (Keil, 2000), and general regolith formation (Housen et al., 1979; Delbo et al., 2014), and they are also of interest for developing space-based economies and resource utilization systems (Metzger et al., 2013; Mueller et al., 2016; Pohl and Britt, 2017; Mardon and Zhou, 2019; Nadoushan et al., 2020; Srivastava et al., 2023). Asteroids are too small to have atmospheres and also too small to drive internal heat generation processes after the earliest period of Solar System accretion (Housen et al., 1979) so it can be assumed that any regolith present is formed from thermal disintegration, irradiation, collisional events with impactors ranging in size from micrometeorites to other asteroids, and aqueous alteration (Housen et al., 1979; Housen and Wilkening, 1982; Clark et al., 2002; Che and Zega, 2023). A group of asteroids of great scientific and resource-based interest are the C-complex asteroids, which are thought to include some of the most primitive bodies in the Solar System and the source of the well-characterized carbonaceous chondrite meteorites (Johnson and Fanale, 1973; Rivkin, 2012). This group includes subtypes which are close in chemical composition to the Sun and the primitive solar nebula and often have water- and other volatile-enriched minerals (Brearley, 2006; King et al., 2015). The C-complex asteroids contain carbon in addition to phyllosilicates, oxides, and sulfides (Brearley, 2006), and the CI (volatile-rich), CM (moderately enriched in volatiles), and CR (lesser volatile enrichment) carbonaceous chondrites serve as the best source of information on the mineralogy of these volatile-rich asteroid materials (Britt et al., 2019). Understanding the mineralogies and volatile content that are anticipated on the surface of asteroids, and how these parameters drive spectral and physical/thermophysical properties, is key to developing asteroid focused resource and exploration technologies.

Exolith Lab produces three standardized asteroid regolith simulants, based on the mineralogy and physical properties of the carbonaceous chondrites (Britt et al., 2019): CI-V2 (Figure 1I), CM-V2 (Figure 1J), and CR-V2 (Figure 1K). The nomenclature for these simulants deviates from other Exolith Lab naming schemes so that the simulants are not implied to simulate differing degrees of aqueous alteration, such as "CM2". As outlined in Britt et al. (2019), the CI-V2 simulant is based on the mineralogy of the CI chondrite group, specifically the well-characterized Orgueil (Bland et al., 2004), CM-V2 is designed based on the Murchison meteorite (Howard et al., 2009), and CR-V2 is based on the average of five Antarctic CR chondrites (PCA 91082, LAP 02342, QUE 99177, and GRA 06100). It should be noted that the asteroid regolith simulants presented here are created using the "future update" compositions (hence the "V2" designations), rather than the "prototype" compositions given in Britt et al. (2019). Some mineralogical components of the meteorites, such as the Fe-rich serpentine cronstedtite and tochinilite are not common on Earth, so other phyllosilicates (the non-asbestiform, Mg-rich serpentines antigorite or lizardite) and sulfates are used. Each of CI-V2, CM-V2, and CR-V2 are offered, as denoted by Britt et al. (2019), as "dry powder" [≤1,000 μm; coarse sand or finer by Wentworth (1922)] or "cobble" [variable sizes; coarse pebbles or finer by Wentworth (1922)] mixes. The "dry" mixes are simply mixes of the different mineral constituents, processed to size as needed, then mixed together and packaged. These pebble-sized (Wentworth, 1922) simulants are intended to mimic the coherent strength of the pebbles on asteroid surfaces and rubble pile asteroids (Britt et al., 2019) and are produced by binding the finer (coarse sand) mix particles together. For CI-V2, a 1:4 ratio of water to dry mix (by mass) is created and air dried. The resulting solid material, bound together by the clays, loses all added water upon drying and matches strength measurements from CI chondrites (Britt et al., 2019; Metzger et al., 2019; Pohl and Britt, 2020). CM-V2 and CR-V2 have considerably lower clay content that CI-V2, so to make the relatively stronger pebbles from these two dry mixes, sodium metasilicate pentahydrate is dissolved in water, and this solution is mixed in a similar 1:4 ratio as the CI-V2 water binding process, then cured in a block-shaped mold at ~75°C. When stronger pebble-sized aggregates are desired, the concentration of sodium metasilicate can be increased. It has been shown that most of the water added is outgassed during curing and that the sodium metasilicate increases the SiO_2 and Na_2O content of the simulant

TABLE 1 Mineralogical compositions in mass percentages of Exolith Lab lunar regolith simulants LHS-1, LMS-1, LHS-1D, and LMS-1D.

Component	LHS-1 wt%	LMS-1 wt%	LHS-1D wt%	LMS-1D wt%
Anorthosite	74.4	19.8	74.4	19.8
Glass-rich basalt	24.7	32.0	24.7	32.0
Ilmenite	0.4	4.3	0.4	4.3
Olivine	0.2	11.1	0.2	11.1
Pyroxenite (bronzitite)	0.3	32.8	0.3	32.8

TABLE 2 Bulk chemistry of major and minor elements, in equivalent oxides, of the Exolith Lab lunar, Martian, and asteroid regolith simulants as measured by fused bead XRF and the measured loss on ignition (LOI) for each simulant.

Oxide	LHS-1 wt%	LMS-1 wt%	LHS-1D wt%	LMS-1D wt%	MGS-1 wt%	MGS-1C wt%	MGS-1S wt%	JEZ-1 wt%	CI-V2 wt%	CM-V2 wt%	CR-V2 wt%
SiO_2	49.12	48.22	48.67	47.42	43.90	43.83	32.60	38.57	26.44	28.19	36.54
Al_2O_3	26.29	12.40	26.23	14.02	12.84	10.42	9.59	7.87	4.31	3.64	2.43
CaO	13.52	7.65	13.41	8.26	7.91	9.13	21.39	5.39	2.61	3.14	1.89
Na_2O	2.55	1.73	2.51	1.72	1.49	1.48	1.08	0.96	0.09	1.43	1.64
FeO*	3.20	8.79	3.73	8.74	10.60	7.34	7.79	8.34	23.24	13.39	27.62
MgO	2.86	15.97	2.66	14.91	14.81	13.47	11.51	26.96	24.04	30.61	25.18
MnO	0.06	0.2	0.06	0.18	0.112	0.09	0.087	0.10	0.06	0.04	0.16
TiO_2	0.63	2.70	0.70	2.68	0.46	0.39	0.361	0.29	0.41	0.26	0.14
K_2O	0.34	0.42	0.37	0.39	0.29	1.44	0.32	0.35	0.49	0.03	0.15
P_2O_5	0.17	0.23	0.17	0.20	0.17	0.14	0.125	0.10	0.14	0.10	0.05
LOI	0.41	0.56	0.46	0.48	4.90	10.38	10.76	8.79	16.08	16.86	1.34
Total	99.15	98.87	98.97	99.00	97.48	98.11	95.61	97.73	97.90	97.69	97.14

*Cumulative FeO and Fe_2O_3. The fused bead XRF, methodology does not allow for determination of relative amounts of Fe_2O_3 and FeO so total iron content is reported as FeO.

by less than 2 wt% (Britt et al., 2019). The particle size distribution and range of the pebble-sized simulant varies from batch to batch and is able to be customized per customer needs.

3 Results and discussion

3.1 Lunar regolith simulants

3.1.1 Mineralogy and implications

Since mineralogical accuracy is a cornerstone of the Exolith Lab design philosophy, lunar simulant mineralogy (Table 1) is based on returned samples of a lunar regolith. LHS-1, a lunar highlands simulant is dominantly felsic in nature, mimicking pristine sample mineralogy around the Apollo 16 landing site in the equatorial intercrater highlands as well as around the lunar south pole, the region of interest for of NASA's Artemis program and related missions around the world. LHS-1D has the same mineralogical makeup as LHS-1 just with a reduced particle size, so it is also a mineralogically accurate lunar highlands dust simulant. LMS-1, the Exolith Lab lunar mare simulant, was developed to mimic the mineralogy of pristine and representative returned samples from the lunar mare. Likewise, LMS-1D is a mineralogically accurate lunar mare dust simulant with fidelity inherited from LMS-1.

3.1.2 XRF analysis applications and implications

Knowledge of the bulk elemental composition of lunar regolith simulants used to test technologies such as molten regolith electrolysis (MRE) and sintering in Earth-based laboratories is critical to predicting the performance of the technology on the lunar surface (Sibille et al., 2009; Humbert et al., 2022). Despite the inherent differences in the chemical properties of simulants and lunar regolith (Isachenkov et al., 2022), a mineralogically and geochemically accurate simulant is required to properly develop lunar systems. Once a quantitative understanding of a given lunar ISRU process is established in the lab, the differences in the chemistry of the simulant and actual lunar regolith will be able to be modeled and the system adapted to function more efficiently once deployed on the Moon. Considering this, the elemental abundances of major and minor element equivalent oxides detected by XRF of Exolith Lab lunar regolith simulants produced in February 2023 (and are not expected to undergo any feedstock changes in the coming years) are given in Table 2 and trace

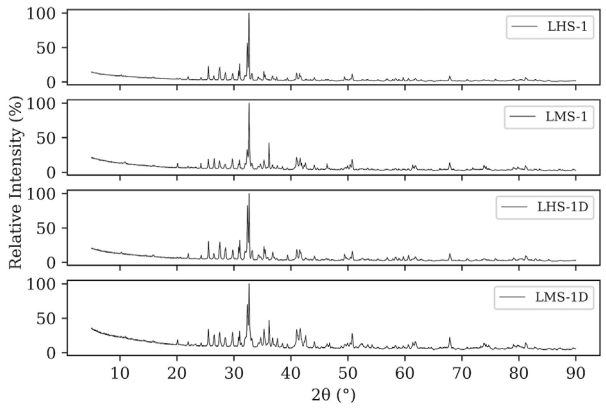

FIGURE 3
X-ray diffraction patterns of Exolith Lab lunar regolith simulants LHS-1, LMS-1, LHS-1D, and LMS-1D obtained using a cobalt cathode with a 2θ wavelength (λ) of 1.79 Å.

element concentrations for these simulants are given in Supplementary Material.

3.1.3 XRD analysis applications and implications

Mineralogy controls the physical and chemical properties of geologic materials, hence having data to characterize the phases present in lunar regolith and lunar simulants allows for better understanding of challenges and requirements for resource prospecting, acquisition, processing, and utilization as well as comparisons between data from surface operations and from in-lab testing. See Long-Fox et al. (2023) for a tabular comparison of the composition of Exolith Lab LHS-1 and LMS-1 simulant versus lunar highlands and mare regolith. The phases present in lunar regolith and lunar regolith simulants, including volcanically-derived glasses, (simulated) agglutinates, and impact melts (in the case of actual lunar regolith) will affect the mechanical strength of the regolith or simulant and how it behaves in high-temperature processes such as microwave or solar sintering and MRE. Since mineralogy underpins every interaction with lunar regolith and its simulants, characterization of the phases present is essential to developing and understanding of how to best develop technologies to leverage local resources on the lunar surface. Therefore, XRD patterns of Exolith Lab lunar regolith simulants LHS-1, LMS-1, LHS-1D, and LMS-1D are given in Figure 3 and data files (2θ angle and counts) are available upon request to the corresponding author.

3.1.4 Particle size analysis applications and implications

Particle size distributions and ranges are a major contributing factor in the geomechanical properties of lunar regolith and its simulants, so technologies developed involving lunar material transport, flow, storage, and processing need to consider particle size range and particle size distribution as a key parameter in testing. The combination of mineralogical accuracy and sample-based (Graf, 1993) particle sizes and particle size distributions of Exolith Lab's LHS-1 and LMS-1 simulants makes them appropriate for terrestrial research and development of lunar resource acquisition, transport, and processing systems (Isachenkov et al., 2022; Long-Fox et al., 2023). The particle size cumulative distribution and density function (both with 2σ confidence intervals) for these specific batches of LHS-1, LMS-1, LHS-1D, and LMS-1D produced in February 2023 are given in Figure 4 and the D10, D30, D50, D60, and D90 percentile values and corresponding distribution spans and uniformity and curvature coefficients are given in Table 3.

3.2 Martian regolith simulants

3.2.1 Mineralogy and implications

The Exolith Lab design philosophy starts with mineralogy, hence MGS-1, MGS-1C, MGS-1S, and JEZ-1 are all based on *in situ* data from Rocknest in Gale crater with some adaptations based on remote sensing data (Cannon et al., 2019). MGS-1 was created to be a global average simulant for Martian regolith in geochemical and geomechanical testing of Martian exploration and infrastructure development systems (Cannon et al., 2019), though it should be noted that the composition of MGS-1 was updated slightly from the original compositions given in Cannon et al. (2019). Since MGS-1C, MGS-1S, and JEZ-1 all use MGS-1 as the base material, remote sensing data was used to provide constraints for each of these simulant constituents beyond the base MGS-1 formula (e.g., Baird et al., 1976; Poulet et al., 2008). The basaltic mineral content (plagioclase, olivine, pyroxenes) was scaled accordingly to simulate localized alterations superimposed onto the base basaltic component. The mineralogical compositions of MGS-1, MGS-1C, MGS-1S, and JEZ-1 produced in February 2023 with no feedstock changes expected over the next few years are given in Table 4.

3.2.2 XRF analysis applications and implications

The bulk elemental composition of a Martian regolith simulant is key information to be considered when designing systems to utilize the Martian regolith for processes such as oxygen and metal extraction, agriculture systems, and other infrastructure. Just as with lunar regolith and lunar regolith simulants described in this work, there are inherent differences in the chemical properties of the Martian regolith and its simulants due to the simulant material being terrestrially derived. Given these differences, thorough investigations must be performed to understand and optimize Martian regolith resource utilization. Before this predictive analysis can happen for the research and development of Martian SRU and exploration systems, testing must first be done in the lab using appropriate simulants. Given the importance of knowing elemental abundances of a simulant for testing across a variety of disciplines, the abundances of major element equivalent oxides of Exolith Lab Martian regolith simulants MGS-1, MGS-1C, MGS-1S, and JEZ-1 detected by XRF are given in Table 2, and the trace element data are given in Supplementary Material.

3.2.3 XRD analysis applications and implications

The mineralogic composition of Martian regolith is highly complex due to the dynamic processes that have been, or are still, active on the Martian surface (Yen et al., 2005; Poulet et al., 2008; Murchie et al., 2009; Bish et al., 2013). Martian regolith simulants must reasonably match the phase compositions measured from robotic sampling operations performed on Mars

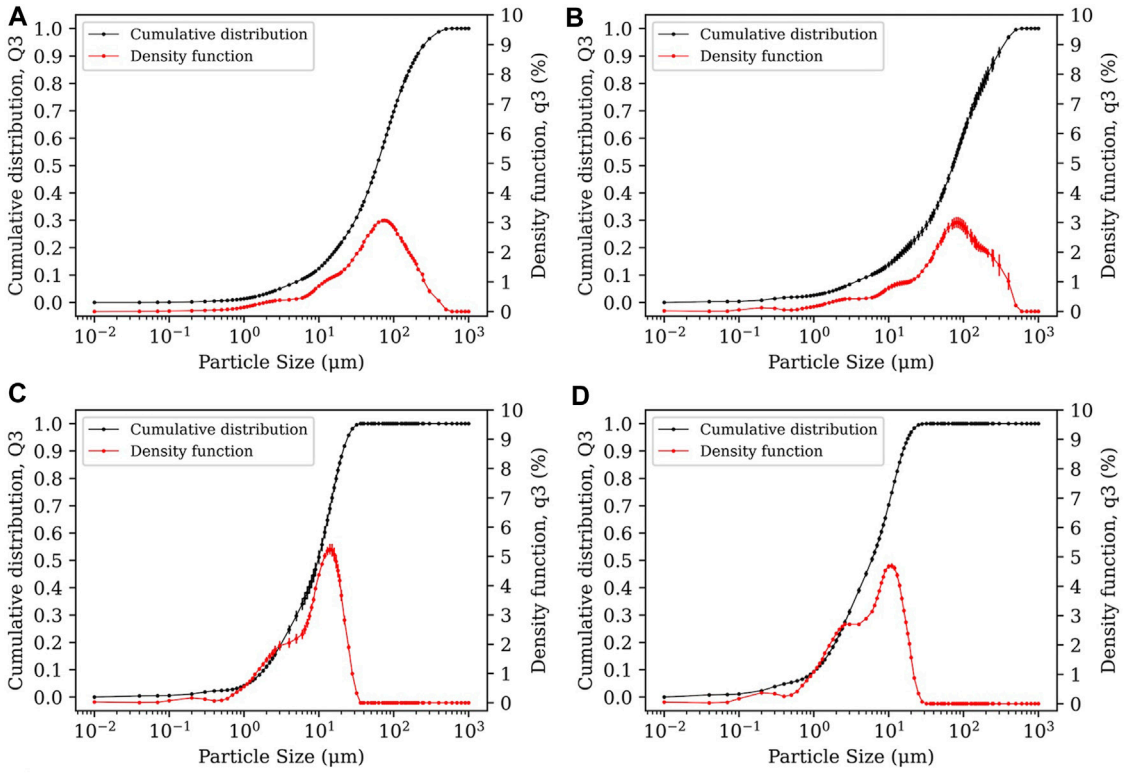

FIGURE 4
Particle size distribution plots of **(A)** LHS-1, **(B)** LMS-1, **(C)** LHS-1D, and **(D)** LMS-1D showing the mean cumulative distribution (Q3) and the density function (q3) of the samples tested with 2σ error bars.

TABLE 3 Percentile values, spans, and gradation coefficients (C_u and C_c) of the particle size distributions of LHS-1, LMS-1, LHS-1D, and LMS-1D lunar regolith simulants.

Quantity	LHS-1	LMS-1	LHS-1D	LMS-1D
D10 (μm)	7.61	5.82	1.85	1.07
D30 (μm)	30.64	35.31	5.08	2.88
D50 (μm)	59.79	72.27	9.74	5.92
D60 (μm)	77.60	95.31	11.94	7.91
D90 (μm)	202.35	282.47	21.06	15.58
Span (dimensionless)	3.26	3.83	1.97	2.45
C_u (dimensionless)	10.20	16.38	6.45	7.39
C_c (dimensionless)	1.59	2.25	1.17	0.98

(Cannon et al., 2019). The high mineralogical diversity of Mars means that there are many different rocks and minerals that can be used in construction and resource extraction for human and autonomous infrastructure development and habitation on Mars, each having a unique set of use cases. Having quantitative data for compositional phases of Martian regolith simulants used in the research and development of Martian-aimed technologies gives the ability to compare and contrast Martian ISRU process sensitivities to compositional variations and hence predict best methodologies for use in flight missions (Cannon et al., 2019). XRD patterns for Martian regolith simulants MGS-1, MGS-1C, MGS-1S, and JEZ-1 are shown in Figure 5 and the data files (2θ angle and counts) are available upon request from the corresponding author.

3.2.4 Particle size analysis applications and implications

As previously stated, the particle size distribution of planetary regolith and simulants are dominant factors that determine the geomechanical properties of the simulant and also affects chemical and thermal processing; this, of course, is also true for Martian regolith simulants. The cumulative distribution and density function (with 2σ confidence intervals) for MGS-1, MGS-1C, MGS-1S, and JEZ-1 are shown graphically in Figure 6 with, and the D10, D30, D50, D60, and D90 percentile values, spans, and coefficients of uniformity and curvature are given in Table 5.

3.3 Asteroid regolith simulants

3.3.1 Mineralogy and implications

Exolith Lab uses mineralogy as the basis of its asteroid simulants, so the mineralogy of Orgueil (Bland et al., 2004), Murchison (Bland et al., 2004), and Antarctic meteorites PCA 91082, GRA 95229, LAP 02342, QUE 99177, GRA 06100 (Howard et al., 2015) are used as reference materials for CI-V2, CM-V2, and CR-V2, respectively, with CR-V2 being based on the Antarctic CRs. As previously stated, the unique mineralogies of asteroids compared to the relatively

TABLE 4 Mineralogical compositions in mass percentages of Exolith Lab Martian regolith simulants MGS-1, MGS-1C, MGS-1S, and JEZ-1.

Component	MGS-1 wt%	MGS-1C wt%	MGS-1S wt%	JEZ-1 wt%
Anhydrite	1.7	1.0	1.0	1.0
Anorthosite	27.1	16.4	16.4	16.0
Fe-carbonate (siderite)	1.4	0.8	0.8	0.8
Ferrihydrite	3.5	2.1	2.1	2.1
Glass-rich basalt	22.9	13.7	13.7	13.5
Gypsum	0.0	0.0	40.0	0.0
Hematite	0.5	0.3	0.3	0.3
Hydrated silica	3.0	1.8	1.8	1.8
Magnetite	1.9	1.1	1.1	1.1
Mg-carbonate	0.0	0.0	0.0	11.0
Mg-sulfate (epsomite)	4.0	2.4	2.4	2.4
Olivine	13.7	8.2	8.2	32.0
Pyroxenite (bronzitite)	20.3	12.2	12.2	12.0
Smectite (montmorillonite)	0.0	40.0	0.0	6.0

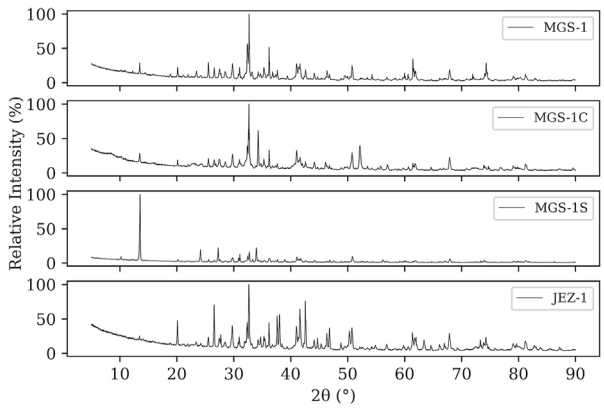

FIGURE 5
X-ray diffraction patterns of Exolith Lab Martian regolith simulants MGS-1, MGS-1C, MGS-1S, and JEZ-1 obtained using a cobalt cathode with a 2θ wavelength (λ) of 1.79 Å.

evolved and oxidized materials on Earth, are not always able to be replicated and substitutions had to be made (e.g., Mg-serpentine substituting for Fe-serpentine). These substitutions that deviate from the expected compositions of asteroidal regolith are judged to be reasonable given the trades and sacrifices of fidelity involved in using a cost-effective, open-source approach to produce large amounts of simulant (Britt et al., 2019). The formulae given in Table 6 for CI-V2, CM-V2, and CR-V2 are the "future updates" referred to in Britt et al. (2019).

3.3.2 XRF analysis applications and implications

Just as with lunar and Martian regolith simulants, the bulk elemental composition of an asteroid regolith simulant must be reasonably accurate to the regolith being simulated to serve as appropriate materials for the testing of various space resource chemical processing systems (Britt et al., 2019; Metzger et al., 2019). Since the exact composition of planetary regolith is impossible to perfectly recreate from terrestrial materials (which are generally enriched in Mg and Al with lesser amounts of Fe), any differences must be quantified and accounted for, which is recommended to be the subject of future publications. For Exolith Lab asteroid regolith simulants, one of the main differences between asteroid regolith and the simulant is the use of Mg-rich, non-asbestiform serpentines as opposed to the Fe-rich cronstedtite (not widely available) and Fe-rich tochilinite (not widely available) being substituted for other Fe-rich compounds such as iron powder. This relative depletion in Fe and enrichment in Mg, while not ideal, offers the best constrained maximization approximation of asteroidal materials while maintaining product availability, safety, and fidelity (Britt et al., 2019). The abundances of major elements in CI-V2, CM-V2, and CR-V2, detected by fused-bead XRF, are given in Table 2 and the trace element concentrations are given in Supplementary Material.

3.3.3 XRD analysis applications and implications

Asteroid regolith is mineralogically complex, and even though asteroids are some of the most primitive bodies in the Solar System and give unique views into Solar System and planetary formation, they are generally modified through radiation bombardment, impacts, and sometimes aqueous alteration. The degree and type of space weathering experienced by asteroids determines how the original mineralogy was altered, and knowledge of phases (altered and unaltered, glassy and crystalline) present in asteroid regolith can provide information on resource potential and on what is required for safe and efficient resource acquisition and extraction processes, anchoring, traversal, excavation, and processing. Such knowledge must be gained in the laboratory using appropriate simulants in research and development (Metzger et al.,

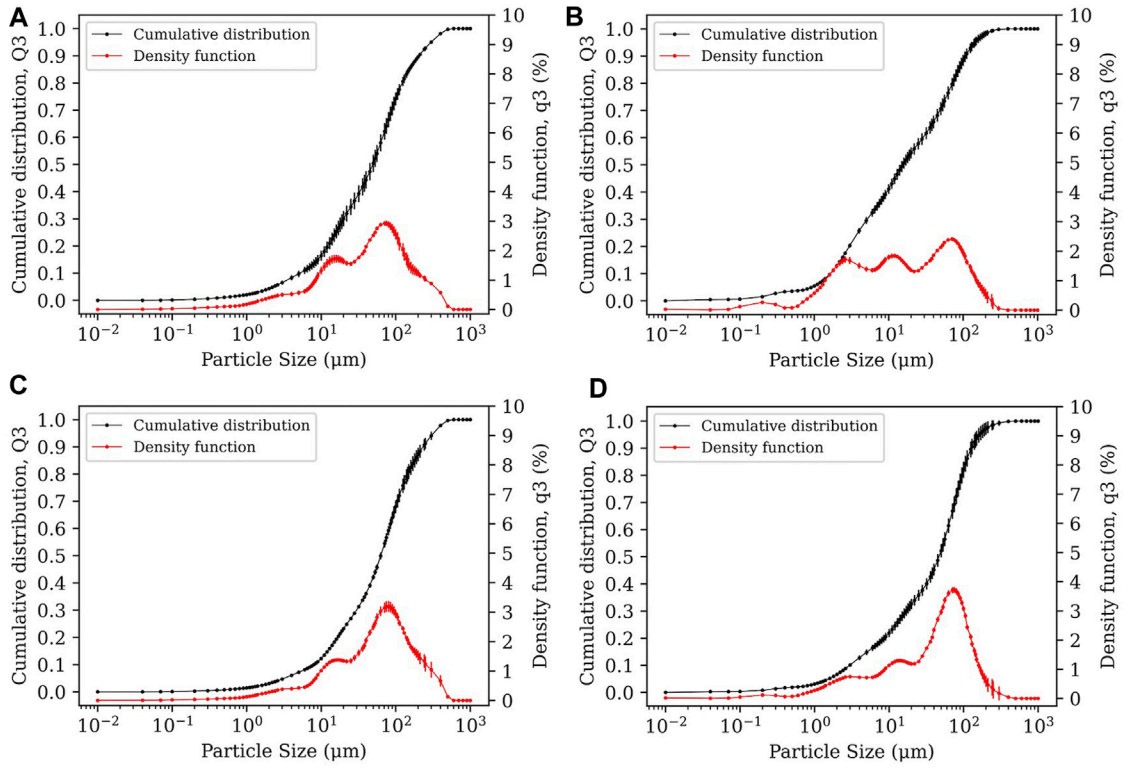

FIGURE 6
Particle size distribution plots of **(A)** MGS-1, **(B)** MGS-1C, **(C)** MGS-1S, and **(D)** JEZ-1 showing the mean cumulative distribution (Q3) and the density function (q3) of the samples tested with 2σ error bars.

TABLE 5 Percentile values, spans, and gradation coefficients (C_u and C_c) of the particle size distributions of MGS-1, MGS-1C, MGS-1S, and JEZ-1 Martian regolith simulants.

Quantity	MGS-1	MGS-1C	MGS-1S	JEZ-1
D10 (μm)	5.19	1.64	7.99	2.97
D30 (μm)	19.96	5.16	29.89	16.91
D50 (μm)	49.30	15.50	63.13	46.92
D60 (μm)	66.85	28.98	81.61	60.99
D90 (μm)	205.48	107.48	233.17	127.27
Span (dimensionless)	4.06	6.83	3.57	2.65
C_u (dimensionless)	12.88	17.67	10.21	20.53
C_c (dimensionless)	1.15	0.56	1.37	1.58

2019). Since the mineralogy is so vital to consider when designing and testing hardware and planning flight missions to interact with asteroids (Britt et al., 2019; Metzger et al., 2019), Exolith Lab asteroid regolith simulants CI-V2, CM-V2, and CR-V2 XRD patterns are given in Figure 7 with data files available upon request from the corresponding author. These data allow Exolith Lab asteroid regolith simulant users to compare results of testing resource acquisition and processing systems that involve elevated temperatures or pressures that may alter the mineralogy of the regolith to get a better understanding of process variation and efficiency.

TABLE 6 Mineralogical compositions in mass percentages of Exolith Lab asteroid regolith simulants CI-V2, CM-V2, and CR-V2.

Component	CI-V2 wt%	CM-V2 wt%	CR-V2 wt%
Amorphous silicate	0.0	0.0	9.6
Fe-carbonate (siderite)	0.0	1.0	0.0
Ferrihydrite	4.8	0.0	0.0
Fe metal powder	0.0	0.0	10.6
Magnetite	10.0	5.0	2.5
Mg-serpentine	51.3	73.8	6.8
Olivine	7.0	11.2	33.1
Palygorskite	5.3	0.0	0.0
Pyrite	7.0	3.3	5.8
Pyroxeneite (bronzitite)	0.0	2.1	29.6
Sub-bituminous coal	5.0	3.6	2.0
Vermiculite	9.6	0.0	0.0

3.3.4 Particle size analysis and implications

The particle size distribution of asteroid regolith simulants is a key property that, like any planetary regolith simulant, affects the geomechanical and thermophysical properties of the simulant.

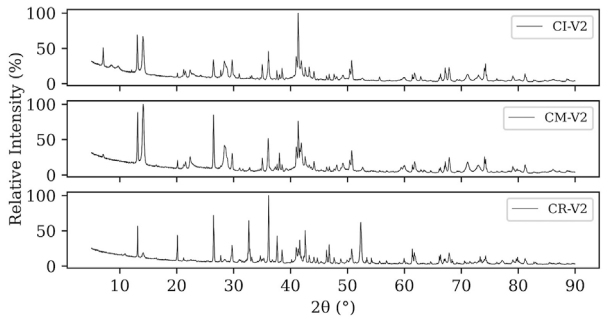

FIGURE 7
X-ray diffraction patterns of Exolith Lab asteroid regolith simulants CI-V2, CM-V2, and CR-V2 obtained using a cobalt cathode with a 2θ wavelength (λ) of 1.79 Å.

TABLE 7 Percentile values, spans, and gradation coefficients (C_u and C_c) of the particle size distributions of CI-V2, CM-V2, and CR-V2 asteroid regolith simulants.

Quantity	CI-V2	CM-V2	CR-V2
D10 (μm)	7.10	5.30	13.71
D30 (μm)	26.67	22.37	48.12
D50 (μm)	48.63	48.21	74.26
D60 (μm)	59.52	63.08	89.21
D90 (μm)	108.36	172.30	251.79
Span (dimensionless)	2.08	3.46	3.21
C_u (dimensionless)	8.38	11.90	6.51
C_c (dimensionless)	1.68	1.50	1.89

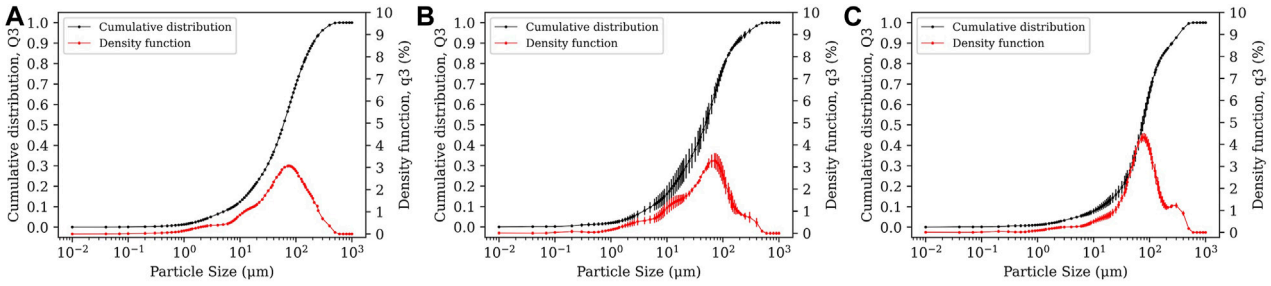

FIGURE 8
Particle size distribution plots of **(A)** CI-V2, **(B)** CM-V2, and **(C)** CR-V2 showing the mean cumulative distribution (Q3) and the density function (q3) of the samples tested with 2σ error bars.

Asteroids themselves are composed of particles from the sub-μm scale to large boulders (e.g., Burke et al., 2021), and as such, CI-V2, CM-V2, and CR-V2 are offered in both powder and a larger pebble-sized (Wentworth, 1922) form, as previously discussed here and in Britt et al. (2019). The laser-based volumetric particle size analysis performed here breaks up the pebbles, so the cumulative distribution and density functions shown in Figure 8 with 2σ confidence intervals and the D10, D30, D50, D60, and D90 percentile values, spans, and gradation coefficients given in Table 7 are only representative of the powder form of each Exolith Lab asteroid regolith simulant. Custom size orders can be placed for pebble-sized simulants if desired by contacting Exolith Lab.

4 Conclusion

Presented here are, at the time of writing, the most up-to-date data on the composition and particle size distributions of Exolith Lab lunar, Martian, and asteroid regolith simulants. Exolith Lab produces lunar, Martian, and asteroid regolith simulants in a constrained optimization of fidelity, safety, and product availability. The design philosophy used in the creation and large-scale production of all Exolith Lab simulants is to start with accurate mineralogy (based on returned samples and/or remote sensing data) and process feedstock to appropriate particle size ranges using industry standard rock and mineral handling equipment. Note that material sources, PSDs, and overall simulant compositions are subject to change due to supplier changes, source material changes, processing equipment changes, or new data that provides improved insights into lunar, Martian, or asteroid regolith. It should also be noted that the PSDs and mineralogic compositions of Exolith Lab simulants may vary from batch to batch and the data provided here are from simulants produced in February 2023. Any of the Exolith Lab simulants are able to be customized to order through free scientific consultation that can be booked at https://www.exolithsimulants.com or sending an email to exolithlab@ucf.edu. Please contact Exolith Lab (HYPERLINK "mailto:exolithlab@ucf.edu" \o "mailto:exolithlab@ucf.edu"exolithlab@ucf.edu or https://www.exolithsimulants.com) for more information on specific simulant batches for the most accurate data available for the given production run.

Data availability statement

The original contributions presented in the study are included in the article/Supplementary Material, further inquiries can be directed to the corresponding author.

Author contributions

JL-F: Conceptualization, Data curation, Formal Analysis, Methodology, Software, Visualization, Writing–original draft,

Writing–review and editing, Investigation. DB: Conceptualization, Funding acquisition, Investigation, Project administration, Resources, Supervision, Writing–review and editing.

Funding

This work was supported by the NASA Solar System Research Virtual Institute (SSERVI) Center for Lunar and Asteroid Surface Science (CLASS) through NASA Cooperative Agreement 80NSSC19M0214.

Acknowledgments

Special thanks go to Dr. Edward Duke and Dr. Jacob Petersen at the South Dakota School of Mines and Technology Engineering and Mining Experiment Station; to Dr. Zach Osborne and Dr. Brandi Langsdorf at the Hamilton College Hamilton Analytical Laboratory. The authors would also like to express our sincerest gratitude to the reviewers for offering kind and useful suggestions that greatly helped improve this manuscript.

Conflict of interest

The authors declare that the research was conducted in the absence of any commercial or financial relationships that could be construed as a potential conflict of interest.

Publisher's note

Supplementary material

The Supplementary Material for this article can be found online at: https://www.frontiersin.org/articles/10.3389/frspt.2023.1255535/full#supplementary-material

References

Achilles, C. N., Downs, R. T., Ming, D. W., Rampe, E. B., Morris, R. V., Treiman, A. H., et al. (2017). Mineralogy of an active eolian sediment from the Namib dune, Gale crater, Mars. *J. Geophys. Res.* 112, 2344–2361. doi:10.1002/2017JE005262

Adler, I., Trombka, J., Gerard, J., Scmadebeck, R., Lowman, P., Blodget, H., et al. (1972a). Apollo 15 geochemical X-ray fluorescence experiment: preliminary report. *Science* 172, 436–440. doi:10.1126/science.175.4020.436

Adler, I., Trombka, J., Gerard, J., Scmadebeck, R., Lowman, P., Blodget, H., et al. (1972b). Apollo 16 geochemical X-ray fluorescence experiment: preliminary report. *Science* 177, 256–259. doi:10.1126/science.177.4045.256

ASTM Standard D2487 (2017). *Standard practice for classification of Soils for engineering purposes (unified soil classification system)*. West Conshohocken, PA: ASTM International.

Baird, A. K., Toulmin, P., Clark, B. C., Rose, H. J., Keil, K., Christian, R. P., et al. (1976). Mineralogic and petrologic implications of viking geochemical results from Mars: interim report. *Science* 194, 1288–1293. doi:10.1126/science.194.4271.1288

Bish, D. L., Blake, D. V., Vaniman, D. T., Chipera, S. J., Morris, R. V., Ming, D. W., et al. (2013). X-ray diffraction results from Mars science laboratory: mineralogy of rocknest at Gale crater. *Science* 341, 1238932. doi:10.1126/science.1238932

Blake, D. F., Morris, R. V., Kocurek, G., Morrison, S. M., Downs, R. T., Bish, D., et al. (2013). Curiosity at Gale crater, Mars: characterization and analysis of the rocknest sand shadow. *Science* 341, 1239505. doi:10.1126/science.1239505

Bland, P. A., Cressey, G., and Menzies, O. N. (2004). Modal mineralogy of carbonaceous chondrites by X-ray diffraction and Mossbauer spectroscopy. *Meteorit. Planet. Sci.* 39, 3–16. doi:10.1111/j.1945-5100.2004.tb00046.x

Brearley, A. J. (2006). "The action of water," in *Meteorites and the early solar system II*". Editors D. S. Lauretta and H. Y. McSween (Tucson, Arizona: The University of Arizona Press), 587–624.

Britt, D. T., Cannon, K. M., Donaldson Hanna, K., Hogancamp, J., Poch, O., Beck, P., et al. (2019). Simulated asteroid materials based on carbonaceous chondrite mineralogies. *Meteorit. Planet. Sci.* 54 (9), 2067–2082. doi:10.1111/maps.13345

Bunaciu, A. A., Udristrioiu, E. g., and Aboul-Enein, H. Y. (2015). X-ray diffraction: instrumentation and applications. *Crit. Rev. Anal. Chem.* 45 (4), 289–299. doi:10.1080/10408347.2014.949616

Burke, K. N., DellaGiustina, D. N., Bennett, C. A., Walsh, K. J., Pajola, M., Bierhaus, E. B., et al. (2021). Particle size-frequency distributions of the OSIRIS-rex candidate sample sites on asteroid (101955) bennu. *Remote Sens.* 13 (7), 1315. doi:10.3390/rs13071315

Cannon, K. M., Britt, D. T., Smith, T. M., Fritsche, R. F., and Batcheldor, D. (2019). Mars global simulant MGS-1: A rocknest-based open standard for basaltic martian regolith simulants. *Icarus* 317, 470–478. doi:10.1016/j.icarus.2018.08.019

Cannon, K. M., Dreyer, C. B., Sowers, G. F., Schmitt, J., Nguyen, T., Sanny, K., et al. (2022). Working with lunar surface materials: review and analysis of dust mitigation and regolith conveyance technologies. *Acta Astronaut.* 196, 259–274. doi:10.1016/j.actaastro.2022.04.037

Carlson, R. W., and Lugmair, G. W. (1979). Sm-Nd constraints on early lunar differentiation and the evolution of KREEP. *Earth Planet. Sci. Lett.* 45 (1), 123–132. doi:10.1016/0012-821X(79)90114-6

Che, S., and Zega, T. Z. (2023). Hydrothermal fluid activity on asteroid Itokawa. *Nat. Astron.* doi:10.1038/s41550-023-02012-x

Clark, B. E., Hapke, B., Pieters, C., and Britt, D. (2002). "Asteroid space weathering and regolith evolution," in *Asteroids II*. Editors R. P. Binzel, T. Gehrels, M. S. Matthews, and A. Tucson (Tucson, Arizona, United States: University of Arizona Press).

Colaprete, A., Andrews, D., Bluethmann, W., Elphic, R. C., Bussey, B., Trimble, J., et al. (2019), "An overview of the volatiles investigating polar exploration rover (VIPER) mission," in American Geophysical Union Fall Meeting, San Francisco, CA, 11-15 December 2023 Abstract #P34B-03.

Crites, S. T., and Lucey, P. G. (2015). Revised mineral and Mg# maps of the Moon from integrating results from the Lunar Prospector neutron and gamma-ray spectrometers with Clementine spectroscopy. *Am. Mineralogist* 100, 973–982. doi:10.2138/am-2015-4874

Delbo, M., Libourel, G., Wilkerson, J., Murdoch, N., Michel, P., Ramesh, K. T., et al. (2014). Thermal fatigue as the origin of regolith on small asteroids. *Nature* 508, 233–236. doi:10.1038/nature13153

Easter, P., Long-Fox, J., Landsman, Z., Metke, A., and Britt, D. (2022). "Comparing the effects of mineralogy and particle size distribution on the angle of repose for lunar regolith simulants," in 53rd Lunar and Planetary Science Conference, Houston, TX, USA, March 7-11, 2022.

Gaddis, L. R., Staid, M. I., Tyburczy, J. A., Hawke, B. R., and Petro, N. E. (2003). Compositional analyses of lunar pyroclastic deposits. *Icarus* 161 (2), 262–280. doi:10.1016/S0019-1035(02)00036-2

Graf, J. C. (1993). Lunar soils grain size catalog. *NASA Ref. Publ.* 1265.

Guerrero-Gonzalez, F. J., and Zabel, P. (2023). System analysis of an ISRU production plant: extraction of metals and oxygen from lunar regolith. *Acta Astronaut.* 203, 187–201. doi:10.1016/j.actaastro.2022.11.050

Gustafson, J. O., Bell, J. F., Gaddis, L. R., Hawke, B. R., and Giguere, T. A. (2012). Characterization of previously unidentified lunar pyroclastic deposits using Lunar Reconnaissance Orbiter Camera data. *J. Geophys. Res. Plan.* 117 (E12). doi:10.1029/2011JE003893

Hagerty, J. J., Lawrence, D. J., Hawke, B. R., Vaniman, D. T., Elphic, R. C., and Feldman, W. C. (2006). Refined thorium abundances for lunar red spots: implications for evolved, nonmare volcanism on the Moon. *J. Geophys. Res. Plan.* 111 (E6), E06002. doi:10.1029/2005JE002592

Haskin, L., and Warren, P. (1991). Lunar chemistry, in *The lunar sourcebook: a user's guide the the moon chapter 8*. Cambridge: Cambridge University Press.

Head, J. W., and McCord, T. B. (1978). Imbrian-age highland volcanism on the Moon: the gruithuisen and mairan domes. *Science* 199 (4336), 1433–1436. doi:10.1126/science.199.4336.1433

Head, J. W., and Wilson, L. (1992). Lunar mare volcanism: stratigraphy, eruption conditions, and the evolution of secondary crusts. *Geochimica Cosmochimica Acta* 56, 2155–2175. doi:10.1016/0016-7037(92)90183-j

Heiken, G., and McKay, D. S. (1974). "Petrography of Apollo 17 soils," in Proc. 5th Lunar Sci. Conference, Houston, Tex., March 18-22, 1974, 843–860.

Hooper, P. R. (1964). Rapid analysis of rocks by X-ray fluorescence. *Anal. Chem.* 36 (7), 1271–1276. doi:10.1021/ac60213a026

Horgan, B. H. N., Anderson, R. B., Dromart, G., Amador, E. S., and Rice, M. S. (2020). The mineral diversity of Jezero crater: evidence for possible lacustrine carbonates on Mars. *Icarus* 339, 113526. doi:10.1016/j.icarus.2019.113526

Hörz, F., Grieve, R., Heiken, G., Spudis, P., and Binder, A. (1991). "Lunar surface processes," in *The lunar sourcebook: A user's guide to the moon" chapter 4* (Cambridge: Cambridge University Press).

Housen, K. R., Wilkening, L. L., Chapman, C. R., and Greenberg, R. (1979). Asteroidal regoliths. *Icarus* 39, 317–351. doi:10.1016/0019-1035(79)90145-3

Housen, K. R., and Wilkening, L. L. (1982). Regoliths on small bodies in the solar system. *Annu. Rev. Earth Planet. Sci.* 10, 355–376. doi:10.1146/annurev.ea.10.050182.002035

Howard, K. T., Alexander, C. M. O'D., Schrader, D. L., and Dyl, K. A. (2015). Classification of hydrous meteorites (CR, CM and C2 ungrouped) by phyllosilicate fraction: PSD-XRD modal mineralogy and planetesimal environments. *Geochimica Cosmochimica Acta* 149, 206–222. doi:10.1016/j.gca.2014.10.025

Howard, K. T., Benedix, G. K., Bland, P. A., and Cressey, G. (2009). Modal mineralogy of CM2 chondrites by X-ray diffraction (PSD-XRD). Part 1: total phyllosilicate abundance and the degree of aqueous alteration. *Geochimica Cosmochimica Acta* 73, 4576–4589. doi:10.1016/j.gca.2009.04.038

Humbert, M. S., Brooks, G. A., Duffy, A. R., Hargrave, C., and Akbar Rhamdhani, M. (2022). Thermophysical property evolution during molten regolith electrolysis. *Planet. Space Sci.* 219, 105527. doi:10.1016/j.pss.2022.105527

Isachenkov, M., Chugunov, S., Landsman, Z., Akhatov, I., Metke, A., Tikhonov, A., et al. (2022). Characterization of novel lunar highland and mare simulants for ISRU research applications. *Icarus* 376, 114873. doi:10.1016/j.icarus.2021.114873

Johnson, D. M., Hooper, P. R., and Conrey, R. M. (1999). XRF analysis of rocks and minerals for major and Trace elements on a single low dilution Li-tetraborate fused Bead. *Adv. X-ray Analysis* 41, 843–867.

Johnson, T. V., and Fanale, F. P. (1973). Optical properties of carbonaceous chondrites and their relationship to asteroids. *J. Geophys. Res.* 78, 8507–8518. doi:10.1029/jb078i035p08507

Jolliff, B. L., Gillis, J. J., Haskin, L. A., Korotev, R. L., and Wieczorek, M. A. (2000). Major lunar crustal terranes: surface expressions and crust-mantle origins. *J. Geophys. Res. Planets* 105 (E2), 4197–4216. doi:10.1029/1999JE001103

Just, G. H., Smith, K., Joy, K. H., and Roy, M. J. (2020). Parametric review of existing regolith excavation techniques for lunar *in Situ* Resource Utilisation (ISRU) and recommendations for future excavation experiments. *Planet. Space Sci.* 180, 104746. doi:10.1016/j.pss.2019.104746

Keil, K. (2000). Thermal alteration of asteroids: evidence from meteorites. *Planet. Space Sci.* 48, 887–903. doi:10.1016/s0032-0633(00)00054-4

King, A. J., Schofield, P. F., Howard, K. T., and Russell, S. S. (2015). Modal mineralogy of CI and CI-like chondrites by X-ray diffraction. *Geochimica Cosmochimica Acta* 165, 148–160. doi:10.1016/j.gca.2015.05.038

Kminek, G., Meyer, M. A., Beaty, D. W., Carrier, B. L., Haltigin, T., and Hays, L. E. (2022). Mars sample return (MSR): planning for returned sample science. *Astrobiology* 22, S-1–S-4. doi:10.1089/ast.2021.0198

Kornuta, D., Abbud-Madrid, A., Atkinson, J., Barr, J., Barnhard, G., Bienhoff, D., et al. (2019). Commercial lunar propellant architecture: A collaborative study of lunar propellant production. *REACH* 13, 100026. doi:10.1016/j.reach.2019.100026

Lemelin, M., Lucey, P. G., and Camon, A. (2022). Compositional maps of the lunar polar regions derived from the kaguya spectral profiler and the lunar orbiter laser altimeter data. *Planet. Sci. J.* 3 (63), 63. doi:10.3847/PSJ/ac532c

Leshin, L. A., Mahaffy, P. R., Webster, C. R., Cabane, M., Coll, P., Conrad, P. G., et al. (2013). Volatile, isotope, and organic analysis of martian fines with the Mars Curiosity rover. *Science* 341, 1238937. doi:10.1126/science.1238937

Long-Fox, J. M., Landsman, Z. A., Easter, P. B., Millwater, C. A., and Britt, D. T. (2023). Geomechanical properties of lunar regolith simulants LHS-1 and LMS-1. *Adv. Space Res.* 71, 5400–5412. doi:10.1016/j.asr.2023.02.034

Madison, A., Landsman, Z., Long-Fox, J., Metke, A., Krol, K., Easter, P., et al. (2022). "Lunar dust simulants and Their applications," in 18th Biennial American Society of Civil Engineers Earth and Space Conference, Denver, CO, USA, 25-28 April 2022.

Malin, M. C., and Edgett, K. S. (2000). Sedimentary rocks of early Mars. *Science* 290, 1927–1937. doi:10.1126/science.290.5498.1927

Mardon, A. A., and Zhou, G. (2019). "Asteroid mining and in-situ mineral resource Utilization," in 82nd Annual Meeting of The Meteoritical Society, Sapporo, held 7–12 July 2019.

McCauley, J. F. (1973). Mariner 9 evidence for wind erosion in the equatorial and midlatitude regions of Mars. *J. Geophys. Res.* 78, 4123–4137. doi:10.1029/JB078i020p04123

McKay, D. S., Carter, J. L., Boles, W. W., Allen, C. C., and Allton, J. H. (1994). JSC-1: A new lunar soil simulant. *Eng. Constr. operations space* 2, 857–866.

McKay, D. S., Heiken, G., Basu, A., Blanford, S. S., Reedy, R., French, B. M., et al. (1991). "The lunar regolith," in *The lunar sourcebook: A user's guide to the moon" chapter 7* (Cambridge: Cambridge University Press).

McKenzie, W., Taylor, G. J., Dera, P., Martel, L. M. V., Lucey, P. G., Hammer, J. E., et al. (2020). "XTRA, A combined XRD/XRF instrument for use in lunar science and resource Utilization," in 51st Lunar and Planetary Science Conference, Houston, TX, USA, March 16–20, 2020.

McSween, H. Y., Jr., Taylor, G. J., and Wyatt, M. B. (2009). Elemental composition of the martian crust. *Science* 324, 736–739. doi:10.1126/science.1165871

Metzger, P. T., Britt, D. T., Covey, S., Schultz, C., Cannon, K. M., Grossman, K. D., et al. (2019). Measuring the fidelity of asteroid regolith and cobble simulants. *Icarus* 321, 632–646. doi:10.1016/j.icarus.2018.12.019

Metzger, P. T., Muscatello, A., Mueller, R. P., and Mantovani, J. (2013). Affordable, rapid bootstrapping of the space industry and solar system civilization. *J. Aerosp. Eng.* 26, 18–29. doi:10.1061/(asce)as.1943-5525.0000236

Millwater, C., Long-Fox, J., Landsman, Z., Metke, A., and Britt, D. (2022). "Direct shear measurements of lunar regolith simulants LHS-1, LHS-1D, LMS-1, and LMS-1D," in 53rd Lunar and Planetary Science Conference, Houston, TX, USA, March 07–11, 2022.

Mueller, R. P., Howe, S., Kochmann, D., Ali, H., Andersen, C., Burgoyne, H., et al. (2016). "Automated additive construction (AAC) for Earth and space using *in-situ* resources," in Proceedings of the Fifteenth Biennial ASCE Aerospace Division International Conference on Engineering, Science, Construction, and Operations in Challenging Environments, Orlando Florida, 11-15 April 2016.

Murchie, S. L., Mustard, J., Ehlmann, B. L., Milliken, R. E., Bishop, J. L., McKeown, N. K., et al. (2009). A synthesis of Martian aqueous mineralogy after 1 Mars year of observations from the Mars Reconnaissance Orbiter. *J. Geophys. Res.* 114, E00D06. doi:10.1029/2009JE003342

Nadoushan, M. D., Ghobadi, M., and Shafaee, M. (2020). Designing reliable detumbling mission for asteroid mining. *Acta Astronaut.* 174, 270–280. doi:10.1016/j.actaastro.2020.05.025

Ohtake, M., Matsunaka, T., Haruyama, J., Yokota, Y., Morota, T., Honda, C., et al. (2009). The global distribution of pure anorthosite on the Moon. *Nature* 461, 236–240. doi:10.1038/nature08317

Pohl, L., and Britt, D. T. (2020). Strengths of meteorites – an overview and analysis of available data. *Meteorit. Planet. Sci.* 55 (4), 962–987. doi:10.1111/maps.13449

Pohl, L., and Britt, D. T. (2017). The radiation shielding potential of CI and CM chondrites. *Adv. Space Res.* 59, 1473–1485. doi:10.1016/j.asr.2016.12.028

Poulet, F., Mangold, N., Loizeau, D., Bibring, J. P., Langevin, T., Michalski, J., et al. (2008). Abundance of minerals in the phyllosilicate-rich units on Mars. *Astron. Astrophys.* 487, L41–L44. doi:10.1051/0004-6361:200810150

Rivkin, A. S. (2012). The fraction of hydrated C-complex asteroids in the asteroid belt from SDSS data. *Icarus* 221, 744–752. doi:10.1016/j.icarus.2012.08.042

Rose, H. J., Cuttitta, F., Dwornik, E. J., Carron, M. K., Christian, R. P., Lindsay, J. R., et al. (1970). Semimicro X-ray fluorescence analysis of lunar samples. *Proc. Apollo 11 Lunar Sci. Conf.* 2, 1493–1497.

Sanders, G., Kleinhenz, J., and Linne, D. (2022). *NASA plans for* in situ *resource utilization (ISRU) development, demonstration, and implementation*. Available at: https://ntrs.nasa.gov/api/citations/20220008799/downloads/NASA%20ISRU%20Plans_Sanders_COSPAR-Final.pdf.

Schmitt, H. H., Lofgren, G., Swann, G. A., and Simmons, G. (1970). "The Apollo 11 samples: introduction," in Proceedings of the Apollo 11 Lunar Science Conference, Houston, TX., held 5-8 January, 1970.

Sibille, L., Carpenter, P., Schlagheck, R., and French, R. A. (2006). *Lunar regolith simulant materials: Recommendations for standardization, production, and usage*. Washington, D.C., United States: NASA. Technical Publication TP2006214605.

Sibille, L., Sadoway, D. R., Sirk, A., Tripathy, P., Melendez, O., Standish, E., et al. (2009). "Recent advances in scale-up development of molten regolith electrolysis for oxygen production in support of a lunar Base," in 47th AIAA Aerospace Sciences Meeting Contribution, Orlando, Florida, 05 January 2009 - 08 January 2009.

Siegler, M. A., Feng, J., Lehman-Franco, K., Andrews-Hanna, J. C., Economos, R. C., St. ClairMillionHead, M. C. J. W., et al. (2023). Remote detection of a lunar granitic batholith at Compton-Belkovich. *Nature* 620, 116–121. doi:10.1038/s41586-023-06183-5

Simon, S. B., Papike, J. J., and Laul, J. C. (1981). The lunar regolith: comparative studies of the Apollo and luna sites. *Petrology soils Apollo 17, Luna 16, 20, 24" Lunar Planet. Sci. Conf. Proc.* 12, 371–388.

Spudis, P., and Pieters, C. (1991). "Global and regional data about the Moon," in *The lunar sourcebook: A user's guide to the moon" chapter 10* (Cambridge: Cambridge University Press).

Srivastava, S., Pradhan, S. S., Luitel, B., Manghaipathy, P., and Romero, M. (2023). Analysis of Technology, economic, and legislation readiness levels of asteroid mining industry: A Base for the future space resource Utilization missions. *New Space* 2023, 21–31. doi:10.1089/space.2021.0025

Sutter, B., McAdam, A. C., Mahaffy, P. R., Ming, D. W., Edgett, K. S., Rampe, E. B., et al. (2017). Evolved gas analyses of sedimentary rocks and eolian sediment in Gale crater, Mars: results of the curiosity rover's sample analysis at Mars instrument from yellowknife bay to the namib dune. *J. Geophys. Res.* 122, 2574–2609. doi:10.1002/2016JE005225

Taylor, G. J., Martel, L. M. V., Lucey, P. G., Gillis-Davis, J. J., Blake, D. F., and Sarrazin, P. (2019). Modal analyses of lunar soils by quantitative x-ray diffraction analysis. *Geochimica Cosmochimica Acta* 266, 17–28. doi:10.1016/j.gca.2019.07.046

Taylor, G. J., Warren, P., Ryder, G., Delano, J., Pieters, C., and Lofgren, G. (1991). "Lunar rocks," in *The lunar sourcebook: A user's guide to the moon" chapter 6* (Cambridge: Cambridge University Press).

Taylor, L. A., Pieters, C. M., Keller, L. P., Morris, R. V., and McKay, D. S. (2001). Lunar mare soils: space weathering and the major effects of surface-correlated nanophase Fe. *J. Geophys. Res.* 106, 27985–27999. doi:10.1029/2000je001402

Thangavelautham, J., and Xu, Y. (2022). The design of autonomous robotic Technologies for lunar launch and landing pad (LLP) preparation. *IEEE Aerosp. Conf.* doi:10.1109/AERO53065.2022.9843755

Toon, O. B., Pollack, J. B., and Sagan, C. (1977). Physical properties of the particles composing the Martian dust storm of 1971-1972. *Icarus* 30, 663–696. doi:10.1016/0019-1035(77)90088-4

Trang, D., Gillis-Davis, J. J., Lemelin, M., Cahill, J. T. S., Hawke, B. R., and Giguere, T. A. (2017). The compositional and physical properties of localized lunar pyroclastic deposits. *Icarus* 283, 232–253. doi:10.1016/j.icarus.2016.09.025

Walsh, K. J., Bierhaus, E. B., Lauretta, D. S., Nolan, M. C., Ballouz, R., Bennett, C. A., et al. (2022). Assessing the sampleability of bennu's surface for the OSIRIS-rex asteroid sample return mission. *Space Sci. Rev.* 218 (20), 20. doi:10.1007/s11214-022-00887-2

Watanabe, S., Hirabayashi, M., Hirata, N., Hirata, N., Noguchi, R., Shimaki, Y., et al. (2019). Hayabusa2 arrives at the carbonaceous asteroid 162173 ryugu—a spinning top–shaped rubble pile. *Science* 364 (6437), 268–272. doi:10.1126/science.aav8032

Wentworth, C. K. (1922). A scale of grade and class Terms for clastic sediments. *J. Geol.* 30 (5), 377–392. doi:10.1086/622910

Wieczorek, M. A., and Phillips, R. J. (2000). The 'procellarum KREEP Terrane': implications for mare volcanism and lunar evolution. *J. Geophys. Res. Plan.* 105 (E8), 20417–20430. doi:10.1029/1999JE001092

Yada, T., Abe, M., Okada, T., Nakato, A., Yogata, K., Miyazaki, A., et al. (2022). Preliminary analysis of the Hayabusa2 samples returned from C-type asteroid Ryugu. *Nat. Astron.* 6, 214–220. doi:10.1038/s41550-021-01550-6

Yen, A. S., Gellert, R., Clark, B. C., Ming, D. W., King, P. L., Schmidt, M. E., et al. (2013). "Evidence for a global martian soil composition extends to Gale Crater," in Proceedings of the Lunar and Planetary Science Conference, March 7–11, 2022.

Yen, A. S., Gellert, R., Schröder, C., Morris, R. V., Bell, J. F., III, Knudson, A. T., et al. (2005). An integrated view of the chemistry and mineralogy of martian soils. *Nature* 436, 49–54. doi:10.1038/nature03637